CGI Delay Compensation

Richard E. McFarland

Ames Research Center
Moffett Field, California

TABLE OF CONTENTS

SUMMARY

Computer-generated graphics in real-time helicopter simulation produces objectionable scene-presentation time delays. In the flight simulation laboratory at Ames Research Center, it has been determined that these delays have an adverse influence on pilot performance during aggressive tasks such as nap-of-the-Earth (NOE) maneuvers.

Using contemporary equipment, computer generated image (CGI) time delays are an unavoidable consequence of the operations required for scene generation. However, providing that magnitude distortions at higher frequencies are tolerable, delay compensation is possible over a restricted frequency range. This range, assumed to have an upper limit of perhaps 10 or 15 rad/sec, conforms approximately to the bandwidth associated with helicopter handling qualities research.

A compensation algorithm is introduced here and evaluated in terms of tradeoffs in frequency responses. The algorithm has a discrete basis and accommodates both a large, constant transport delay interval and a periodic delay interval, as associated with asynchronous operations.

INTRODUCTION

Flight simulation research at the Ames facility includes various computer, motion base, and subsystem configuration options. Either an electro-mechanical camera/model board device, or a Singer-Link CGI system are available for scene presentation. Despite an adequate bandwidth capacity for helicopter research, the model-board's display leaves something to be desired because of its restricted field of view. In contrast, the multi-window CGI, while manifesting minor deficiencies in scene content and texture, is valuable for pilot cues. However, owing to delays in the transmission of position and orientation information, CGI frequency responses are degraded within the operational bandwidth of the pilot.

The Singer-Link CGI system operates asynchronously with a host computer, although the "time of data transfer" is tagged by an accompanying interrupt signal. Data flows sequentially through three CGI processors: (1) the Perkin-Elmer Computer, (2) the Frame Calculator, and (3) the Scan Line Processor. This flow is outlined in figure 1. The processors have the following functions:

Perkin-Elmer Computer

The P-E computer is also called the scene management computer. One of its functions includes the collecting of mathematical descriptions of objects to be used in the scene which requires extensive data retrieval from disc storage. The arrival of new position and orientation data in the P-E computer is accompanied by an interrupt signal; however, scene management proceeds with previous data at a 30 Hz rate.

Frame Calculator

The Frame Calculator is also called the geometric processing computer, or digital image generator (DIG). Geometric processing is the conversion of mathematical descriptions of three-dimensional data base objects into two dimensions, as associated with the coordinates at the display.

Scan Line Processor

The Scan Line Processor is also called the video processor. It performs the steps necessary to define the image at each picture element (including considerations of occlusion), and generates the video display signals.

When these processors perform their required functions, a time delay occurs between the commanded presentation of the host computer and the actual display. This delay consists of "a pure transport delay" component plus a "periodic" component, which are quantified herein. The discrete nature of these delay sources suggests that a compensation scheme also have a discrete (rather than continuous) basis. This is the approach used here. Whenever possible, the results are displayed using conventional parametric representations, such as magnitude and phase diagrams.

THROUGHPUT

The major component of time delay is the workload required to perform the above processes. This workload is equivalent to the CGI system throughput:

"... the system throughput (defined as the time it takes to complete a scene after the parameters of the viewpoint become available) must be so fast that the delay does not distract the observer. The commonly used update requirement is 100 msec" (ref. 1).

"Throughput" is pure transport delay. However, other components of time delay also exist in simulation; the sum of these components degrades simulation fidelity.

Delay Sources

Five sources of time delay in discrete simulation are identified in this section. Two of these, pure transport delay and periodic delay, are the major causes of CGI response degradation.

Time delay due to discrete realization— When the discrete sample rate is high compared to the frequency content delivered by the model, phase differences between continuum and discrete representations are generally small. Equivalent time delays are functions of frequency, and over some bandwidth may actually produce lead rather than lag, depending upon the discrete parameters. This influence is relatively negligible for a "sufficiently band-limited" system (ref. 2), such as that assumed here.

Loiter delay— In the context of this paper, loiter delay does not exist. Quoted values for loiter delay, on the order of 20 msec, indicate that it is usually identified with the mean value of the P-E computer's asynchronous operational delay, more properly given as 16.67 msec. However, this quantity is not significant here; the host computer's I/O cycle time T actually determines the frequency distribution function of the delay, and it is periodic rather than random. Periodic delay is handled below, and includes this "loiter" contribution.

There is some evidence that a small transmission delay (which might be called loiter delay) of approximately 6 msec exists in our facility configuration (ref. 3), but this value is so small that it is ignored here.

Pure transport delay— The P-E Processor, the Frame Calculator, and the Scan Line Processor operate in parallel at 30 Hz. However, information flows serially through each of these components because of their pipeline architecture. Scene presentation thus occurs 100 msec after information utilization (not acceptance) by the P-E computer. This delay

value is constant, and is given here by T_C; it is the major source of CGI response degradation.

Periodic delay— Asynchronous operation of a CGI processor with respect to a host computer produces a time delay that appears to be random, but is actually periodic. Harmonics of this delay may also be present, depending upon the host computer cycle time T. Periodic delay, given here by $T_A(m)$, varies at a 30-Hz rate. (This will be discussed under Maximum Time Delay.)

Zero-order hold delay— Because of the 30-Hz data refresh rate of CGI monitors, scenes are presented in accordance with the zero-order hold phenomenon, with an average equivalent time delay of 16.67 msec. When this phenomenon is considered along with the electronics of continuous scan line generation by the video processor, which also has an average time delay of 16.67 msec, the net result is a pure transport delay of 33.33 msec. The zero-order hold delay may thus be ignored when the total value of 33.33 msec is attributed to the Scan Line Processor.

SCENE PRESENTATION DELAY

Figure 1 outlines the relevant processes in the CGI loop for the purpose of examining scene presentation delays which are caused by pure transport delay and periodic delay. The host computer produces data each T, which is assumed to be correctly synchronized with real time, and immediately transferred (neglecting any residual loiter delay) to the P-E buffer (X). As shown in figure 1, this transfer is accompanied by an interrupt signal. This Data-Ready Interrupt (DRI) is transmitted by the host computer each I/O cycle time T, and accompanied by the data buffer X. The interrupt is serviced by the P-E computer without interfering with current operations on the extant buffer Y. The data buffer X replaces the data buffer Y every 33.33 msec within the P-E computer.

Sample Rate Conversion

Determining the maximum value of periodic time delay for an arbitrary host-computer cycle time T requires a numerical analysis based upon least common multiples. For cycle times restricted to integer multiples of milliseconds, the analysis proceeds as follows:

The host computer produces a signal $x(n)$ sampled at the rate $F = 1/T$, and the P-E computer observes the signal $y(m)$ sampled at the rate $F' = 1/T'$. Where N and M are integers, the ratio of sampling periods may be expressed as a rational fraction:

$$T'/T = F/F' = M/N \qquad (1)$$

The ratios of integers (M/N) will be seen to be important in the following material. Using the P-E's sample rate of 30 Hz, equation (1) becomes

$$(33.33...)/T = 100/(3T) = M/N \qquad (2)$$

where T is an integer number of milliseconds. Given that N is the *least common divisor* in equation (1), it may be shown (ref. 4) that the system response is periodic in m with period N. The *period of time delay* is thus given by

$$P = NT' = N/30 \quad (\text{sec}) \qquad (3)$$

when the fraction given by equation (2) has been reduced to its lowest terms, i.e. M and N are relatively prime (to each other). Values for M and N over a wide range of host-computer cycle times T are shown in tables 1 and 2. For example, when $T = 60$ msec equation (2) reduces to $M/N = 5/9$. In the range of host computer cycle times from one to 70 msec the period P may be as small as 0.1 sec (e.g., when $T = 50$ msec), or as large as 100 times the host computer's cycle time (e.g., 6.9 sec for $T = 69$ msec). The period of time delay is given in figure 2(a), where the cycle time T of the host computer is an integer number of milliseconds. Harmonics of this period also occur for various cycle times.

Maximum Time Delay

Both the maximum and average scene presentation time delays are shown in figure 2(b), as a function of cycle time. This figure illustrates the discontinuous behavior of the asynchronous system as a function of its primary parameter, T.

The data in figure 2(b) agree with measured data acquired in a previous study (ref. 5), but this analysis draws a slightly modified conclusion. Paulk reports a linear relationship between T and lag, but it is shown here that only to a first approximation does a linear relationship exist between the visual time delay and the cycle time. Also, the additional computer cycle of the reference (a technique of measurement) is not pertinent. Without compensation of any sort, the model/CGI average time delay may be approximated by 100 msec plus one-half of the cycle time of the host computer; but for 50 msec, for instance, this is a very pessimistic approximation. It is assumed that the host computer will transmit the correct command as synchronized with real time; otherwise the results are distorted by the discrete integration algorithms. This assumption is not invalidated if the drive signal is a control input of the pilot. Inputs, which are generally force or moment proportional, may be assumed to be correctly integrated within the host computer.

The periodic component of time delay may be written analytically. At the 30-Hz rate, where "time" may be given as $t = m/30$ sec (within the P-E computer), the periodic delay component is given by

$$T_A(m) = T_A(m + N) = T\left\{ m/(30T) - \lfloor m/(30T) \rfloor \right\} \qquad (4)$$

In this expression the half brackets ($\lfloor \ \rfloor$) denote the least integer operation. The interval of time $T_A(m)$ constitutes the "projection interval" over which the P-E computer calculates extrapolated positions by use of the products of velocity times $T_A(m)$. This projection operation will be discussed further once the subject of compensation is introduced. (See "Projection.")

The total time delay in the asynchronous system of figure 1 has the periodic component given in equation (4). The minimum time delay is the pure transport delay $T_C = 100$ msec, while the maximum time delay is given by $T_C + T_A(m)$, where m increments at 30-Hz. Time delays as functions of cycle time are illustrated in figures 3(a) through 3(l) for cycle times in the range of 49 to 60 msec (each msec). The fundamental period of time delay is also shown in each of these figures, and agrees with values previously given in figure 2(a) for a large range of cycle times. Harmonics are also observed for certain cycle times. The maximum value for $T_A(m)$ is less than the cycle time T, and the average value is one-half the maximum value. These facts are demonstrated in the Appendix. Tables 1 and 2 are provided for clarification. In these tables the value m(max) is the value of m when $T_A(m)$ achieves its maximum value over the period P.

From the above it is concluded that total time delay is *always less* than the sum of cycle time plus pure transport delay.

MODEL TRANSFER FUNCTION

In this section a second-order transfer function is developed that approximates specific aircraft behavior; in simulation this behavior was recently used to identify delay problems in CGI responses. This transfer function is selected as a basis for the study of the asynchronous logic of figure 1.

Scene presentation delays have been identified as causing degradation related to erroneous pilot cues in the XV-15 (Tilt Rotor, UH-60A) simulation model, (ref. 6) especially in roll response (ref. 7). For the purpose of simplification, an approximate second-order system is used in this analysis. The system closely matches the observed hover response of the XV-15 in the roll axis. The second-order system has the natural frequency $\omega = 7.259$ rad/sec and damping $\xi = 0.4547$. Using these parameters, the continuous response of the model is shown as a parametric curve in both figures 4(a) and 4(b). The discrete equivalent of this system is also given at the specific cycle time of 60 msec.

In order to convert the system into an equivalent discrete model, the specific integration algorithms (ref. 8) used at Ames Research Center have been used, and are given here in z-transform notation. These algorithms consist of the Adams'

3

second-order integration formula for the acceleration-to-velocity integration (a predictor),

$$I_1(z) = \frac{(T/2)(3z - 1)}{z(z - 1)} \qquad (5)$$

and the trapezoidal formula for the velocity-to-position integration (a corrector).

$$I_2(z) = \frac{(T/2)(z + 1)}{z - 1} \qquad (6)$$

By using these algorithms and defining the parameters,

$$
\begin{aligned}
A &= \omega T \\
a_0 &= (4\zeta - A)A \\
a_1 &= 2A^2 - 16\zeta A + 4 \\
a_2 &= 3A^2 + 12\zeta A - 8
\end{aligned}
\qquad (7)
$$

the discrete system response function (z transform) is produced:

$$F(z) = \frac{A^2(3z^2 + 2z - 1)}{4z^3 + a_2 z^2 + a_1 z + a_0} \qquad (8)$$

Magnitude and phase responses of the discrete system given by equation 8 are a function of the cycle time of the host computer T. The resultant curves are tagged "discrete simulation" in figures 4(a) and 4(b), where the cycle time is assumed to be 60 msec; they show that this relatively large cycle time is sufficient (small enough) for the approximation of continuum results for this transfer function out to about 20 rad/sec.

To approximate the influence of CGI time delay on the system $F(z)$, the total phase angles owing to the minimum, average and maximum delays are shown in figure 4(b) as computed by simple algebraic operations. (Time delays do not influence the magnitude responses of figure 4(a), but do produce large phase errors, as shown in figure 4(b)).

Figures 4(a) and (b) have been obtained by using z transforms. They constitute a basis for comparison with other data in this document which has been obtained by use of time-series data.

COMPENSATION

In this section, modified position and velocity terms are developed that project positions (and orientations) much further than previous formulations. The assumptions of this projection are such that the entire delay interval is accommodated, with good frequency response characteristics over the entire operational bandwidth. Acceleration terms have been avoided in the development of this algorithm because: 1) they are not concurrent with velocity and position terms in real-time simulation, and 2) their high-frequency components, prior to "airframe attenuation," are not generally consistent with the assumed band-limited behavior.

In the host computer, operations by the integration algorithms (5) and (6) produce the vehicle velocity $v(n)$ and position $u(n)$, which are transmitted to the X buffer of the P-E computer with an accompanying data-ready interrupt signal, as indicated in figure 1. Heretofore, only compensation for the periodic interval $T_A(m)$ has been used because the projection of an interval greater than this value cannot be supported under a purely linear hypothesis. It is known, however, that the additional pure transport delay component T_c of 100 msec also exists prior to scene presentation. Indeed, for less exacting tasks than helicopter research, this delay seems to be generally accepted (ref. 1). Failure to account for this larger delay interval is due to the fact that general delay compensation does not exist. The compensation problem is put in its proper context in the "linear approach" section.

Linear Approach

"Projection" has been defined as the linear extrapolation over $T_A(m)$ that is performed within the P-E computer. The question arises as to the influence of also extrapolating positions over the pure transport delay interval within the host computer. The resultant pure linear compensation for the entire delay interval is here examined in terms of its component parts.

The technique of linearly extrapolating position over the additional pure transport delay interval of 100 msec successfully eliminates the phase angle error given in figure 4(b), but deteriorates the magnitude response of figure 4(a). These phenomena are illustrated in figures 5(a) and 5(b). where the discrete curves were obtained from a statistical analysis of time series data with Gaussian inputs. The time series data was created from a model of the asynchronous logic as shown in figure 1. The use of the unusual cycle time $T = 66.66$ msec is related to the statistical analysis of (what appears to be) a nonstationary system, under the conditions of minimal data acquisition.

Figures 5(a) and (b) each contain four parametric curves in order to illustrate the components of the extrapolation process, and the standard "projection" process. The continuous system curves are identical to those in figures 4(a) and 4(b). The curves labled "discrete, without linear compensation" represent the scene presentation without any attempt at either extrapolation or projection. Since this particular system does not use the standard, linear projection operation of the P-E computer, these curves approximate the average time delay.

As will be discussed under "Model Verification," this average delay is 116.66 msec when $T = 66.66$ msec. The remaining two parametric curves in figures 5(a) and (b) show both the influence of linear extrapolation, or compensation, and the combined influence of linear compensation plus projection. The combined operations thus constitute the direct application of linear terms to the prediction of positional data.

Figure 5(a) illustrates the basic problem encountered when linear compensation is used. As an extension of this approach, the lead-lag technique implies that sufficient lag must be superimposed to attenuate the magnitude error (linearly compensated, with projection) of figure 5(a), while retaining the phase characteristics of figure 5(b). Using linear analysis, recent work has been performed at Ames to "distribute the attendant system gain distortion (over frequency) so as to minimize gain-distortion effects on system responsiveness (ω_c), pilot workload, and tracking accuracy (ref. 9)." This approach addresses the pilot-aircraft dynamics in the region of "crossover." The nonlinear, double-tuned algorithm developed here is not an extension of this technique, although the applicable bandwidth is assumed to contain the crossover frequency.

Modified commands are developed below that account for the total delay interval, under assumptions that include tuning increments to both a specified frequency, and to the constant velocity condition. The resultant algorithm will be seen to retain its features in the interval between these discrete assumption points, and thus enhance the quality of position information (both translational and rotational) over the operational bandwidth.

The Tuned Corrector

In this section, a position increment is derived that accounts for the interval of pure transport delay. A sequence of velocity values is assumed available at 100-msec intervals. The compensation scheme is derived from this assumption, plus a selected parametric relationship. In the next section, a technique for approximating the required velocity sequence is given.

Consider the three-parameter, velocity-to-position corrector relationship given by

$$u_{k+1} = u_k + (f_0 v_{k+1} + f_1 v_k + f_2 v_{k-1})T_c \qquad (9)$$

In this expression time t is assumed to be incremented according to

$$t = kT_c \qquad (k = 0,1,2,...) \qquad (10)$$

where T_c is the large transport delay interval of 0.1 sec. In the following material, the "tuned" condition simply means that the stated condition satisfies the assumed relationship (eq. 9). For example, sinusoidal behavior may be described

by substituting $u_k = \exp(jWkT_c)$. When equation (9) is tuned to a specific "cutoff frequency" W, the following two relationships are produced,

$$(f_0 - f_2)\sin U = (1 - \cos U)/U \qquad (11)$$

$$(f_0 + f_2)\cos U + f_1 = \sin U/U \qquad (12)$$

where the cutoff bandwidth is given by

$$U = WT_c \qquad (13)$$

The specific frequency W is defined as the upper limit of some "operational bandwidth." The lower limit of this bandwidth is the zero frequency, or constant velocity condition. By also tuning equation (9) to this condition, the additional relationship

$$f_0 + f_1 + f_2 = 1 \qquad (14)$$

is produced. The simultaneous solution of equations (11), (12) and (14) then produces the intermediate coefficients

$$f_0 = \frac{U \sin U - 2 \cos U(1 - \cos U)}{2 U \sin U(1 - \cos U)} \qquad (15)$$

$$f_1 = \frac{2 \sin U(\sin U - U \cos U)}{2 U \sin U(1 - \cos U)} \qquad (16)$$

$$f_2 = \frac{U \sin U - 2(1 - \cos U)}{2 U \sin U(1 - \cos U)} \qquad (17)$$

Using these coefficients, equation (9) represents the position transition from the point k to the point $k + 1$. By forcing the point k to be coincident with the most recent data observation point of the host computer n, we may write equation (9) as,

$$u_{k+1} = u_n + v'T_c \qquad (18)$$

where the applicable velocity v' for this increment has been given in terms of velocity values that are equally spaced by 100-msec intervals, i.e.,

$$v' = f_0 v_{k+1} + f_1 v_k + f_2 v_{k-1} \qquad (19)$$

A form of this corrector has also been developed using geometric relationships in an application to a system with a known dominant mode. It has been successfully applied to

the integration of aircraft states (ref. 10). In order to apply the corrector to an asynchronous system, however, velocity values symmetrically located about the point k (or n) with interval T must be developed.

Symmetric Data

The point k is defined as the most recent point of data delivery of the host computer. The point $k + 1$ thus defines a point 100 msec in the future, and the point $k - 1$ defines a point 100 msec in the past. Velocity values at these two symmetric data points are estimated in this section using the actual data sequence within the host computer.

In order to create symmetrical data points consistent with the above assumptions, sinusoidal prediction is used. Consider the velocity sequence $\{v_{n-2}, v_{n-1}, v_n\}$ of the host computer, where v_n is the most recent value. In contrast to equation (10), time t is related to the host computer's cycle time T by

$$t = nT \quad (n = 0,1,2,\ldots) \quad (20)$$

A sinusoidal curve fit to the velocity sequence is given in the temporal space of the host computer by

$$v(t - 2T) = g_0 + g_1 \sin[W(t - 2T)] + g_2 \cos[W(t - 2T)] \quad (21)$$

where, for convenience

$$v_{n-2} = v(-2T)$$

$$v_{n-1} = v(-T) \quad (22)$$

$$v_n = v(0)$$

By defining the applicable bandwidth

$$V = WT \quad (23)$$

the curve-fit coefficients may then be given by

$$g_0 = \frac{v_n - 2v_{n-1} \cos V + v_{n-2}}{2(1 - \cos V)} \quad (24)$$

$$g_1 = \frac{(1 + 2 \cos V)v_n - 2(1 + \cos V)v_{n-1} + v_{n-2}}{2 \sin V} \quad (25)$$

$$g_2 = \frac{(1 - 2 \cos V)v_n + 2 v_{n-1} \cos V - v_{n-2}}{2(1 - \cos V)} \quad (26)$$

Using these intermediate coefficients, the symmetric sequence for equation (19) is given by

$$v(T_k) = v_{k+1} = g_0 + g_1 \sin U + g_2 \cos U \quad (27)$$

$$v(0) = v_k = v_n \quad (28)$$

$$v(-T_k) = v_{k-1} = g_0 - g_1 \sin U + g_2 \cos U \quad (29)$$

where U was defined in equation (13).

The Algorithm

In view of the above developments, equation (9) may be converted to a function of the velocity sequence of the host computer,

$$u_{k+1} = u_n + b_0 v_n + b_1 v_{n-1} + b_2 v_{n-2} \quad (30)$$

where applicable coefficients for this difference equation are given by

$$b_0 = \frac{U + \sin U(1 - 2 \cos V)}{2 W(1 - \cos V)} + \frac{(1 - \cos U)(1 + 2 \cos V)}{2 W \sin V} \quad (31)$$

$$b_1 = \frac{(\sin U - U)\cos V}{W(1 - \cos V)} - \frac{(1 - \cos U)(1 + \cos V)}{W \sin V} \quad (32)$$

$$b_2 = \frac{U - \sin U}{2 W(1 - \cos V)} + \frac{1 - \cos U}{2 W \sin V} \quad (33)$$

In addition to estimating position, the velocity at $k + 1$ must be estimated for P-E projection purposes. This may be accomplished by using equations (24) through (27). The velocity that accounts for pure time delay (for later projection purposes) may then also be written in terms of the host-computer velocity history,

$$v_{k+1} = d_0 v_n + d_1 v_{n-1} + d_2 v_{n-2} \quad (34)$$

where the appropriate coefficients are given by

$$d_0 = \frac{1 + (1 - 2 \cos V)\cos U}{2(1 - \cos V)} + \frac{(1 + 2 \cos V)\sin U}{2 \sin V} \quad (35)$$

$$d_1 = \frac{\cos V(\cos U - 1)}{1 - \cos V} - \frac{(1 + \cos V)\sin U}{\sin V} \quad (36)$$

$$d_2 = \frac{1 - \cos U}{2(1 - \cos V)} + \frac{\sin U}{2 \sin V} \qquad (37)$$

Since the b_k and d_k coefficients are constant for a given cycle time, the applicable compensation equations are the simple linear combinations given in equations (30) and (34). They constitute the real time workload of the host computer for each of the position and orientation commands. The workload of the P-E computer is not changed. It consists of extrapolation over the periodic interval, i.e.,

$$u' = u_{k+1} + T_A(m)v_{k+1} \qquad (38)$$

which has the same form as the original P-E algorithm. Note, however, that the symmetrical distribution of time delay about $T_c + T_A(\text{avg})$ suggests that the compensation interval of the algorithm may be further extended to include the average value of periodic delay, with appropriate modification to the projection interval in the software of the P-E computer. Neither this extension nor the technique of accommodating the entire compensation algorithm within the P-E computer are discussed here.

The algorithm is outlined in figures 6(a) and (b). The mainframe operations are shown in figure 6(a), and the P-E operations are shown in figure 6(b). The previously established second-order system is used in figure 6(a) for illustration, along with the standard integration algorithms (5) and (6). In figure 6(b), the "up arrows" refer to sample rate expanders (ref. 4), an operation also referred to as "interpolation." If the host computer cycle time was less than 33.33 msec, these arrows should properly be pointing down in an operation called "decimation." The "expanded" operations are asynchronous with those of figure 6(a), and produce periodic behavior in the quantity $T_A(z,z')$. The z-transform operations referred to by z' have a 30-Hz update rate; the resultant time delay represented by $(z')^{-3}$ is 100 msec.

ASYNCHRONOUS MODEL

For the purpose of computing frequency responses the pertinent asynchronous data flow of the CGI system was modeled. Interrupt logic was emulated by using time increments with the granularity of 1/3 msec. Pertinent mainframe and CGI operations are as outlined in figures 6(a) and (b), where the z and z' transformations refer to different sample intervals, with periodic interaction.

For statistical analyses, a worst-case cycle time of 66.66 msec was selected for two reasons: First, this value approximates the value of 60 msec that was used in recent simulation studies, and is therefore currently relevant.

Second, serious resolution bias errors (ref. 11) are avoided by using a sample rate that is a multiple of the P-E computer speed. Otherwise, the system appears to be nonstationary owing to its extremely long period, and conventional spectral analysis techniques yield dubious estimates of frequency response functions.

Model Verification

Figures 4(a) and (b) were obtained by using z-transforms as convoluted to frequency space, and thus represent a standard for verification of the asynchronous model, which is measured only by use of statistical analysis procedures.

The estimated frequency response functions of figures 7(a) and (b) were obtained from the asynchronous model by using correlation and spectral analysis. Continuum results are also displayed in these figures, and parametric curves are presented from the analysis. In figures 7(a) and (b) the compensation algorithm was not used, so that the P-E computer model received the primary values given by $u(z)$ and $v(z)$ as shown in figure 6(a). Two parametric curves are shown, indicating whether the clock in figure 6(b) was used (with projection) or not (without projection).

The use of cycle time that is a multiple (two) of the cycle time of the P-E computer has minimized distortion in the spectral analysis so that the curves closely approximate the results previously given in figures 4(a) and (b). Using this particular cycle time, phase errors do not vary much from the continuum results owing to the fact that $N = 2$ in equation (2) which results in a maximum $T_A(m) = 33.33$ msec in equation (4). The average projection interval is only 16.66 msec when $T = 66.66$ msec; hence, the phase angle history in figure 7(b) remains close to the "minimum bounddary" given in figure 4(b).

Projection

The "projection" operation of the P-E computer does not appear to enhance performance in figures 7(a) and (b) to any great extent, but this is a misleading observation when viewed in frequency space. The small decrease in phase error is actually quite significant, and the resultant "smoothing" is quite important. Illustrations of this are made by converting to the time domain and using an accelerated sinusoidal drive signal. This particular drive signal illustrates the bandwidth of interest because its frequency ramps from 0 to 20 rad/sec in the displayed interval of 7 sec.

To demonstrate the smoothing phenomenon in temporal space, the traces "without projection" and "with projection" are given in figures 8(a) and (b), respectively, using the accelerated sine wave as described above. The continuum curves are also presented. The cycle time $T = 60$ msec has been used for these functions of time.

7

In terms of scene presentation delay, figure 8(b) represents the current state of the art in CGI technology. It exemplifies the phase problems for frequencies in the bandwidth out to about 20 rad/sec. For high frequencies the projection operation of the P-E computer amplifies signals slightly, but this amplification is minimal, especially when compared to the amplification that accompanies compensation algorithms.

The projection operation of the P-E computer is critical in minimizing the granularity caused by both asynchronous operations and large host computer cycle times. The clock-measured projection interval T_A is as given in both figures 1 and 6(b). Note, however, that the applicable position and velocity signals are modified within the host computer when the compensation algorithm is used. The algorithm does not require changes within the CGI system.

The standard projection operation of the P-E computer is used in all of the following material.

Application of the Algorithm

By using the compensation algorithm, decreases in phase error (or time delay) are accompanied by alterations in magnitude responses. This is demonstrated below by varying the available parameter W which has been defined as the cutoff frequency. A satisfactory W selection is dependent upon the frequency content of the position and velocity data transmitted by the host computer.

Without compensation, the applicable magnitude and phase responses have been given in figures 7(a) and (b) by the particular curves labeled "with projection." The pertinent time response has been given in figure 8(b). These curves are for comparison with the following cases where the compensation algorithm is used.

Using the compensation algorithm, figures 9(a) and (b) are produced. They give the magnitude and phase variations as a function of the parameter W (cutoff frequency). For convenience, the continuous system response is also included in these figures. Figures 10(a) and (b) complete the picture by giving time responses using two values of the selected parameter. From these figures, the tradeoff becomes apparent: If the data is band-limited to 10 or 15 rad/sec, amplification beyond this limit may be ignored, and the algorithm clearly eliminates the objectionable phase error. If higher frequencies are known to exist in the data, the parameter W must be increased with corresponding degradation in the lower frequency region. Although this degradation is not rapid, alternate techniques for attenuating the high-frequency gain may be required in certain applications. Specifically, anti-aliasing or notch filters may be required for blade-element rotorcraft models (ref. 12).

Compensation for time delay is invariably accompanied by magnitude variations. The essential differences between this discretely-designed compensation scheme and continuously-designed schemes are: 1) the concomitant reduction to discrete form is avoided, with its resultant deviation from the design objective; 2) two distinct frequencies are used in the design process, with good characteristics over the associated interval. By defining one distinct frequency as d.c. and the other at 10 or 15 rad/sec, the region of crossover is generally included $(0 < w_c < W)$. Hence, the question of design relative to a particular aircraft or pilot is avoided. As with analogous compensation techniques, the "resulting increase in system gain at frequencies $>w_c$ is not normally a problem, because system amplitude ratio and input and disturbance signal power usually decrease rapidly at frequencies $>w_c$." (ref. 9).

If signal power does indeed decrease rapidly beyond the crossover frequency, additional attenuation is not required. The single parameter W should of course be small with respect to the Nyquist frequency. Since the operational bandwidth of the pilot should also be small with respect to the Nyquist frequency for successful real-time simulation, the optimum placement of W can be at the discretion of the simulation analyst. The results have proven to be relatively insensitive to this parameter.

A typical single-axis dynamic check is shown in figure 11, where the parameter $W = 10$ rad/sec. For these particular real-time simulation traces the required cycle time was 62 msec. In figure 11, the positional lead of approximately 130 msec is observed in the CGI commanded roll angle, as predicted. Also, modifications are apparent in the projection velocity, as transmitted to the CGI system.

A novel experiment was conducted to verify both the existence of time delays, as quantified herein, and the compensation algorithm's ability to eliminate these delays. This experiment used sinesoidal commands over a range of frequencies to drive both an oscilloscope display, and a CGI-created horizon. Various host-computer cycle times were also used. By use of optical beam-splitting techniques the visual signals appeared on the same CGI monitor. Superimposition of these signals was possible by manual adjustment of a phase component in the oscilloscope drive signal. Researchers replicated the standard CGI system's theoretical delay values to within negligible tolerances. Most importantly, they could not identify time delays whenever the compensation algorithm was used.

CONCLUSIONS

A compensation algorithm has been developed that virtually eliminates CGI scene presentation delay for the frequency bandwidth out to about 15 rad/sec, using a worst-case scenario with cycle times in the 60-msec range.

If position and orientation signals are known to be band-limited by this value, the compensation algorithm is applicable without further consideration.

If high-frequency content is known to contaminate the CGI drive signals, further considerations may be necessary such as anti-aliasing or notch filters.

In general, the compensation algorithm described here should enhance CGI performance, and be especially valuable for high-gain tasks such as those required in helicopter simulation.

APPENDIX I

PERIODIC DELAY

The periodic component of CGI time delay may be written

$$T_A(m) = T\{mM/N - \lfloor mM/N \rfloor\}$$

where the half bracket operation denotes the least integer. In this equation the ratio of sample rates

$$T'/T = 1/(30T) = M/N$$

has been expressed in terms of M and N that are relatively prime. The average value for the periodic component of time delay is given by

$$T_A(\text{avg}) = \frac{1}{N} \sum_{m=1}^{N} T_A(m)$$

which may be evaluated using the following relationships. First, when the greatest common divisor of the positive integers M and N is unity we have (ref. 12)

$$\sum_{m=1}^{N} \lfloor mM/N \rfloor = M + (M-1)(N-1)/2$$

and second, we have the trivial summation

$$\sum_{m=1}^{N} m = N(N+1)/2$$

These produce the average periodic delay:

$$T_A(\text{avg}) = (T/N) \sum_{m=1}^{N} \{mM/N - \lfloor mM/N \rfloor\}$$

$$= (T/N)\{(M/N)[N(N+1)/2 - [M(1+N) + 1 - N]\}$$

$$= (T/2)(1 - 1/N)$$

Also, it may be demonstrated that for m on $(1,70)$ the maximum value for $T_A(m)$ is twice the average value. It is conjectured that for all m,

$$T_A(\text{max}) = T(1 - 1/N)$$

which means that the total time delay is never quite as large as the sum of cycle time and pure transport delay.

REFERENCES

1. Erickson, Cliff; Fairchild, Kim M.; and Marvel, Orin: Simulation Gets a New Look. (Computer Generated Synthesis Imagery Development) Defense Electronics, vol. 16, no. 8, Aug. 1984, pp. 76–87.

2. Oppenheim, Alan V.; and Schafer, Ronald W.: Digital Signal Processing. Prentice-Hall, Inc., 1975, pp. 202-203.

3. Cleveland, William B.: A Time Lag Study of the Vertical Motion Simulator Computer System. NASA TM-81306, Aug. 1981, p. 12.

4. Crochiere, Ronald E.; and Rabiner, Lawrence R.: Interpolation and Decimation of Digital Signals — A Tutorial Review. IEEE Proceedings, vol. 69, no. 3, March 1981, pp. 300–331.

5. Paulk, Clyde H., Jr.; Astill, David L.; and Donley, Shawn T.: Simulation and Evaluation of the SH-2F Helicopter in a Shipboard Environment Using the Interchangeable Cab System. NASA TM-84387, Aug. 1983, pp. 14, 74, 75.

6. Harendra, P. B., Joglekar, M. J.; Gaffey, T. M.; and Marr, R. L.: A Mathematical Model for Real Time Flight Simulation of the Bell Model 301 Tilt Rotor Research Aircraft. NASA CR-114614, April 1973.

7. Churchill, Gary B.; and Dugan, Daniel C.: Simulation of the XV-15 Tilt Rotor Research Aircraft, NASA TM-84222, March 1982, pp. 12-13.

8. McFarland, Richard E.: A Standard Kinematic Model for Flight Simulation at NASA-Ames. NASA CR-2497, Jan. 1975, p. 27.

9. Crane, D. Francis: Compensation for Time Delay in Flight Simulator Visual-Display Systems. AIAA Flight Simulation Technologies Conference Collection of Technical Papers, Niagara Falls, NY, June 1983, pp. 163–171.

10. Rolston, David R.: Sinusoidal Integration for Simulation of Second-Order Systems. AIAA Flight Simulation Technologies Conference Collection of Technical Papers, Niagara Falls, NY, June 1983, pp. 52–63.

11. Bendat, Julius S.; and Piersol, Allan G.: Engineering Applications of Correlation and Spectral Analysis, John Wiley & Sons, 1980, p. 105.

12. McFarland, Richard E.: The N/Rev Phenomenon in Simulating a Blade-Element Rotor System. NASA TM-84344, March 1983, p. 2.

13. Knuth, Donald E.: The Art of Computer Programming. Vol. I, Fundamental Algorithms. 2nd ed. Addison-Wesley, 1973, p. 42.

TABLE 1.—PARAMETERS FOR THE TIME DELAY
Cycle Time Range from 1 to 35 msec

T, msec	M	N	P, sec	m(max)	T_A(max), msec	T_A(avg), msec
1	100	3	0.1	2	0.67	0.33
2	50	3	.1	1	1.33	.67
3	100	9	.3	8	2.67	1.33
4	25	3	.1	2	2.67	1.33
5	20	3	.1	1	3.33	1.67
6	50	9	.3	7	5.33	2.67
7	100	21	.7	17	6.67	3.33
8	25	6	.2	5	6.67	3.33
9	100	27	.9	17	8.67	4.33
10	10	3	.1	2	6.67	3.33
11	100	33	1.1	32	10.67	5.33
12	25	9	.3	5	10.67	5.33
13	100	39	1.3	23	12.67	6.33
14	50	21	.7	13	13.33	6.67
15	20	9	.3	4	13.33	6.67
16	25	12	.4	11	14.67	7.33
17	100	51	1.7	26	16.67	8.33
18	50	27	.9	7	17.33	8.67
19	100	57	1.9	53	18.67	9.33
20	5	3	.1	1	13.33	6.67
21	100	63	2.1	17	20.67	10.33
22	50	33	1.1	31	21.33	10.67
23	100	69	2.3	20	22.67	11.33
24	25	18	.6	5	22.67	11.33
25	4	3	.1	2	16.67	8.33
26	50	39	1.3	7	25.33	12.67
27	100	81	2.7	17	26.67	13.33
28	25	21	.7	5	26.67	13.33
29	100	87	2.9	20	28.67	14.33
30	10	9	.3	8	26.67	13.33
31	100	93	3.1	53	30.67	15.33
32	25	24	.8	23	30.67	15.33
33	100	99	3.3	98	32.67	16.33
34	50	51	1.7	1	33.33	16.67
35	20	21	.7	1	33.33	16.67

TABLE 2.– PARAMETERS FOR THE TIME DELAY
Cycle Time Range from 36 to 70 msec

T, msec	M	N	P, sec	m(max)	T_A(max), msec	T_A(avg), msec
36	25	27	0.9	14	34.67	17.33
37	100	111	3.7	101	36.67	18.33
38	50	57	1.9	49	37.33	18.67
39	100	117	3.9	62	38.67	19.33
40	5	6	.2	1	33.33	16.67
41	100	123	4.1	107	40.67	20.33
42	50	63	2.1	34	41.33	20.67
43	100	129	4.3	89	42.67	21.33
44	25	33	1.1	29	42.67	21.33
45	20	27	.9	4	43.33	21.67
46	50	69	2.3	40	45.33	22.67
47	100	141	4.7	86	46.67	23.33
48	25	36	1.2	23	46.67	23.33
49	100	147	4.9	122	48.67	24.33
50	2	3	.1	1	33.33	16.67
51	100	153	5.1	26	50.67	25.33
52	25	39	1.3	14	50.67	25.33
53	100	159	5.3	62	52.67	26.33
54	50	81	2.7	34	53.33	26.67
55	20	33	1.1	28	53.33	26.67
56	25	42	1.4	5	54.67	27.33
57	100	171	5.7	53	56.67	28.33
58	50	87	2.9	40	57.33	28.67
59	100	177	5.9	23	58.67	29.33
60	5	9	.3	7	53.33	26.67
61	100	183	6.1	86	60.67	30.33
62	50	93	3.1	13	61.33	30.67
63	100	189	6.3	17	62.67	31.33
64	25	48	1.6	23	62.67	31.33
65	20	39	1.3	37	63.33	31.67
66	50	99	3.3	97	65.33	32.67
67	100	201	6.7	2	66.67	33.33
68	25	51	1.7	2	66.67	33.33
69	100	207	6.9	89	68.67	34.33
70	10	21	.7	2	66.67	33.33

PERKIN-ELMER LOOP

DATA-READY INTERRUPT

(30 Hz)

(1/T Hz)

DRI DISABLE

DRI RECEIVED
AND ENABLED

STOP TIMER
READ TIMER: T_A
RESTART TIMER
FROM CURRENT VALUE

STOP TIMER
RESET TIMER
START TIMER

TRANSFER BUFFER
X TO Y

ACCEPT BUFFER X

DRI ENABLE

RETURN TO
INTERRUPT LOCATION
IN P-E LOOP

>0

INTERROGATE
IMODE
FROM Y BUFFER

≤0

COMPUTE
COMPENSATION
$f(Y, T_A)$

$f(Y, T_A) = 0$

COMPUTE DESIRED PRESENTATION
$Z = Y + f(Y, T_A)$

(30 Hz)

FRAME CALCULATOR

(30 Hz)

SCAN LINE PROCESSOR

Figure 1.— Asynchronous data flow.

14
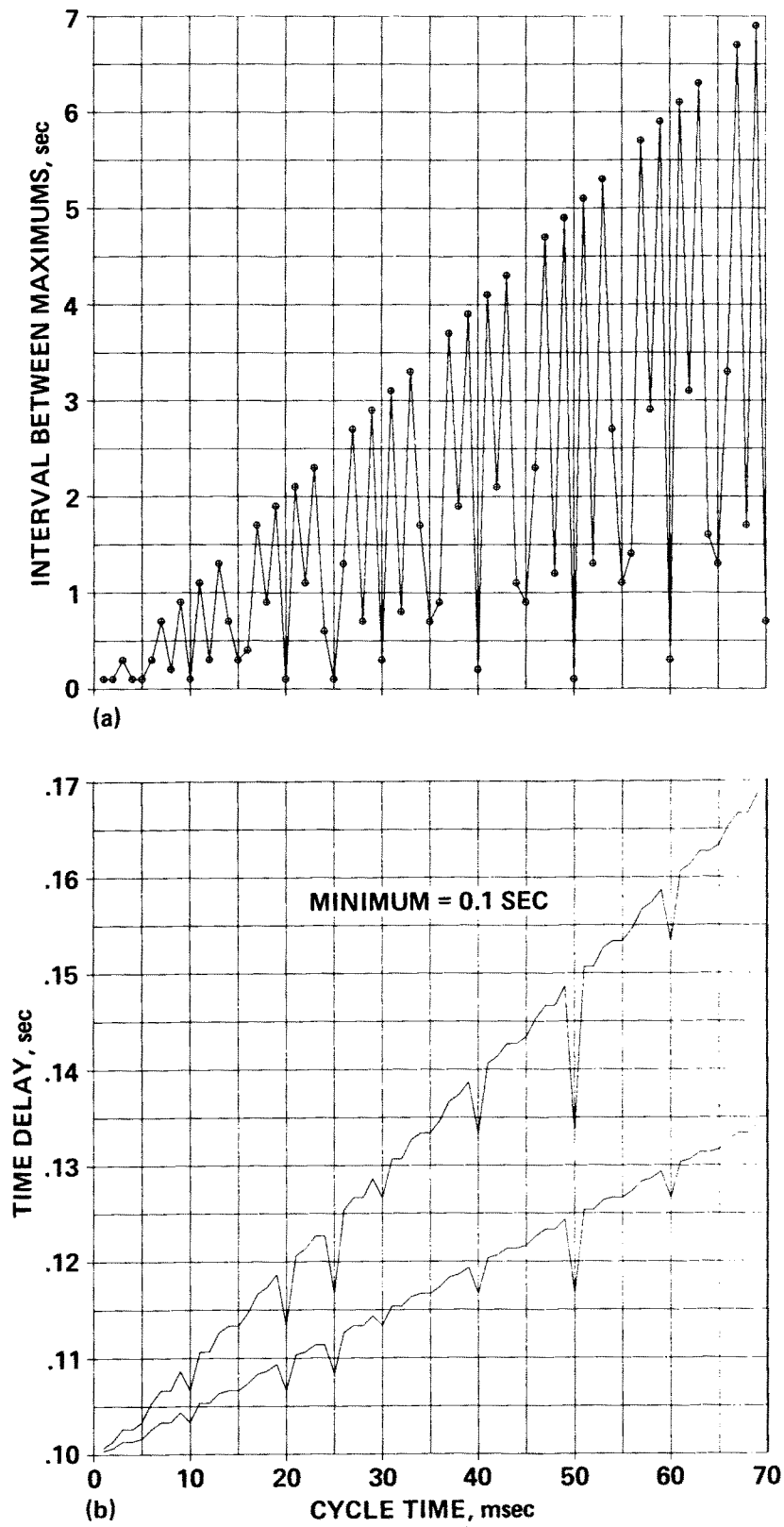
Figure 2.— Time delay characteristics. (a) Period of time delay. (b) Maximum and average delay.
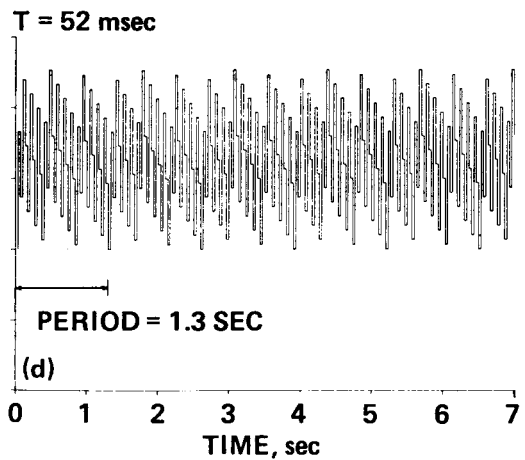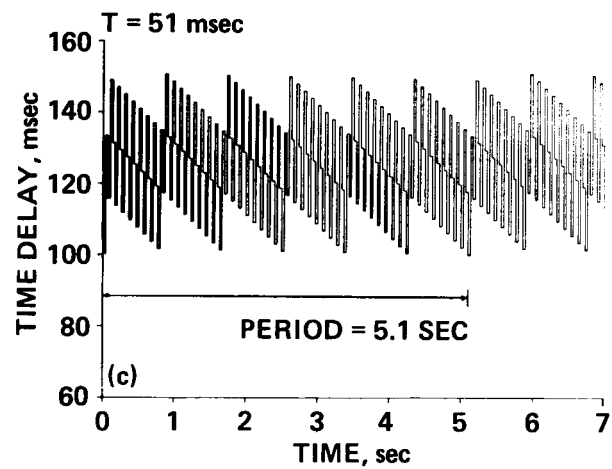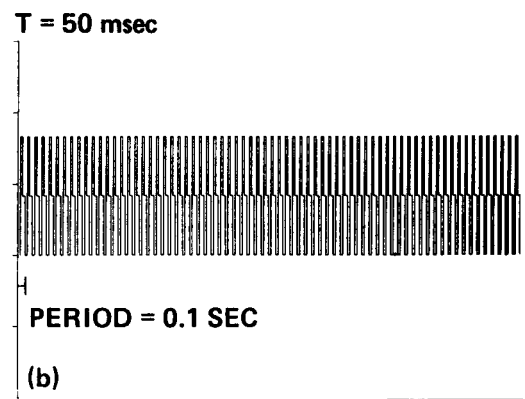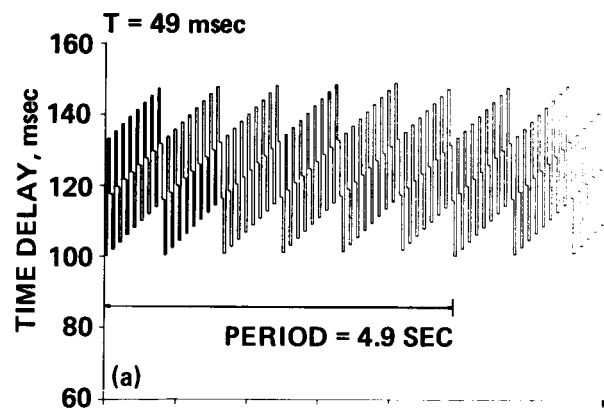
Figure 3.– Scene presentation delays. (a) Cycle time of 49 msec. (b) Cycle time of 50 msec. (c) Cycle time of 51 msec. (d) Cycle time of 52 msec.

16
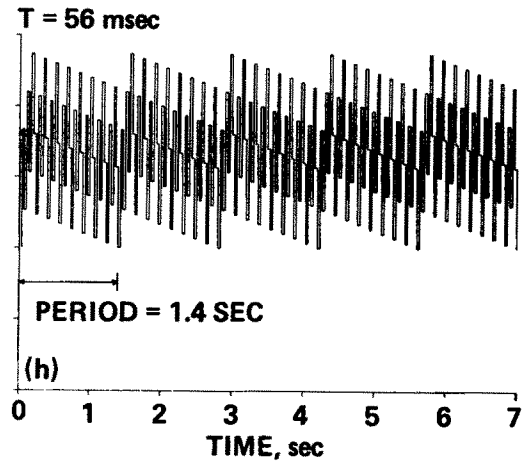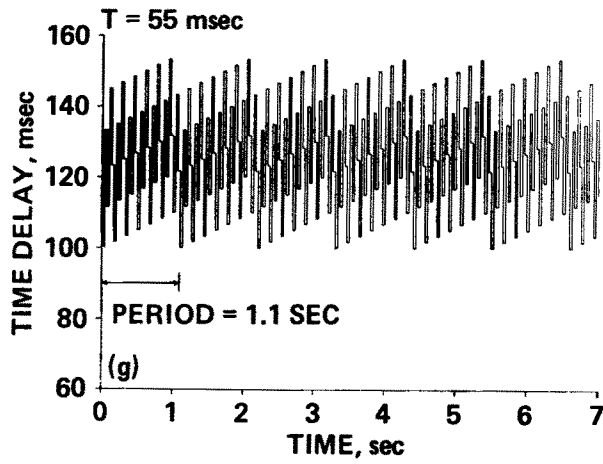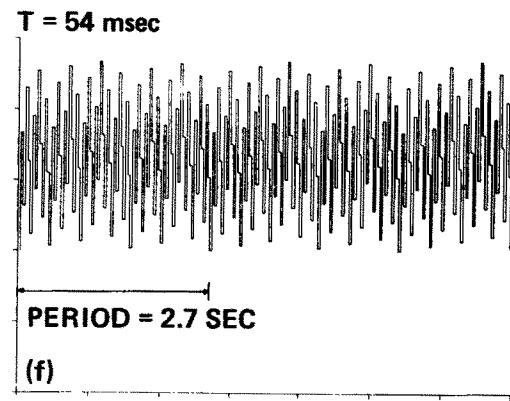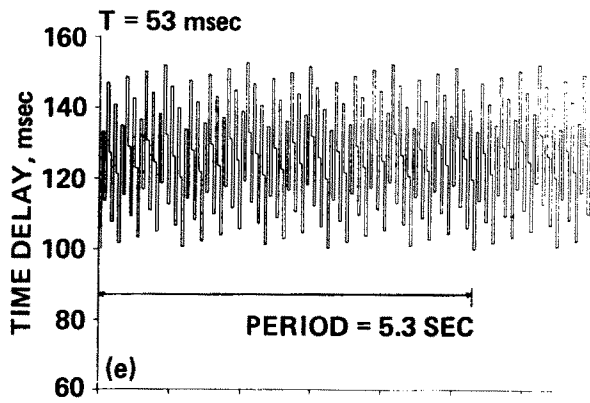
Figure 3.— Continued. (e) Cycle time of 53 msec. (f) Cycle time of 54 msec. (g) Cycle time of 55 msec. (h) Cycle time of 56 msec.
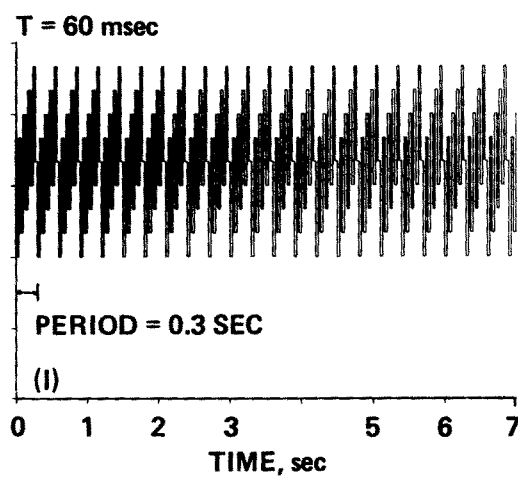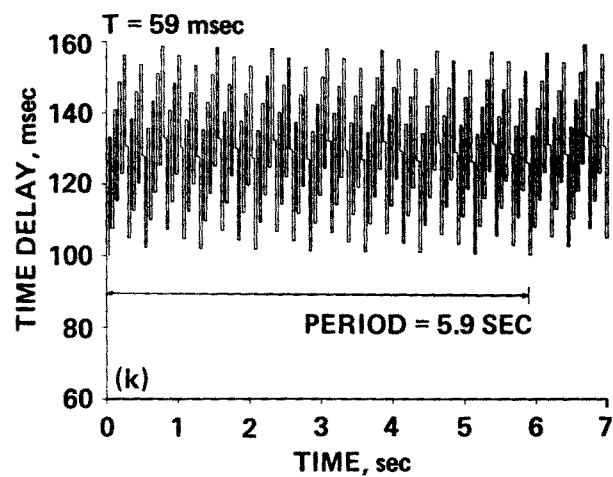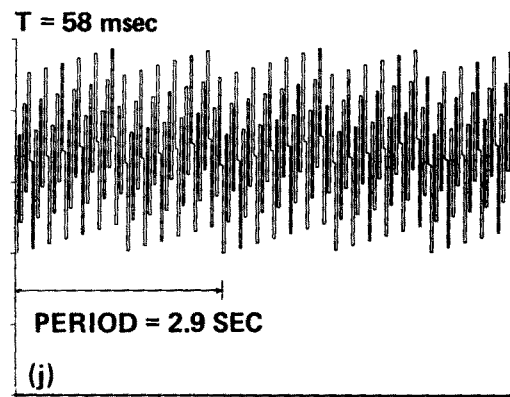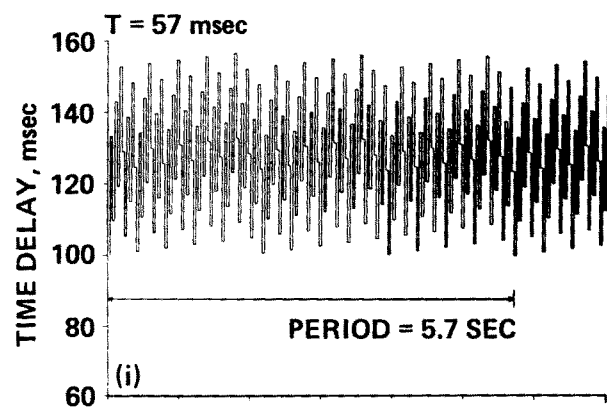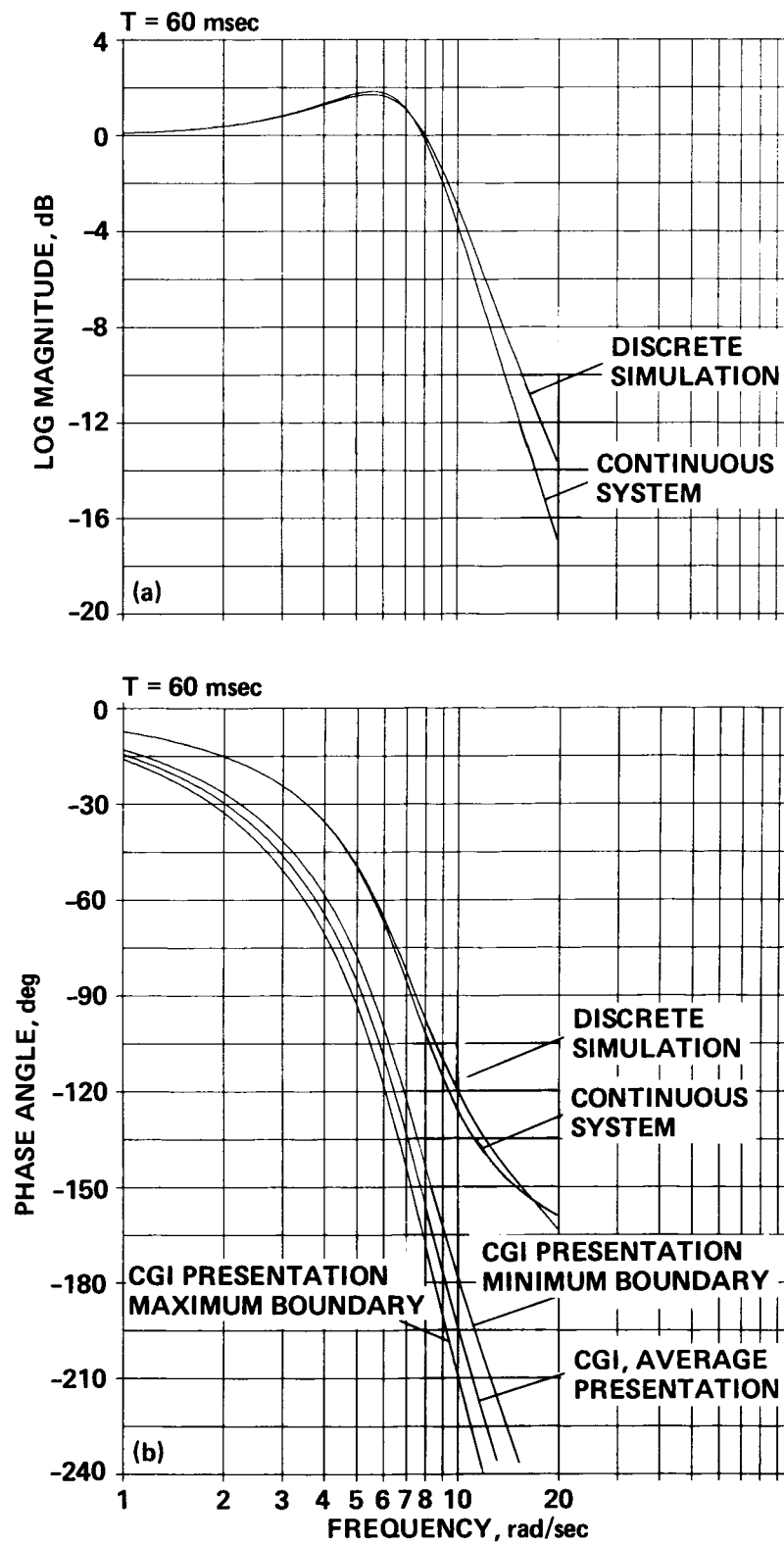
Figure 3.— Concluded. (i) Cycle time of 57 msec. (j) Cycle time of 58 msec. (k) Cycle time of 59 msec. (l) Cycle time of 60 msec.

Figure 4.— Continuous and discrete transfer function. (a) Magnitude. (b) Phase.
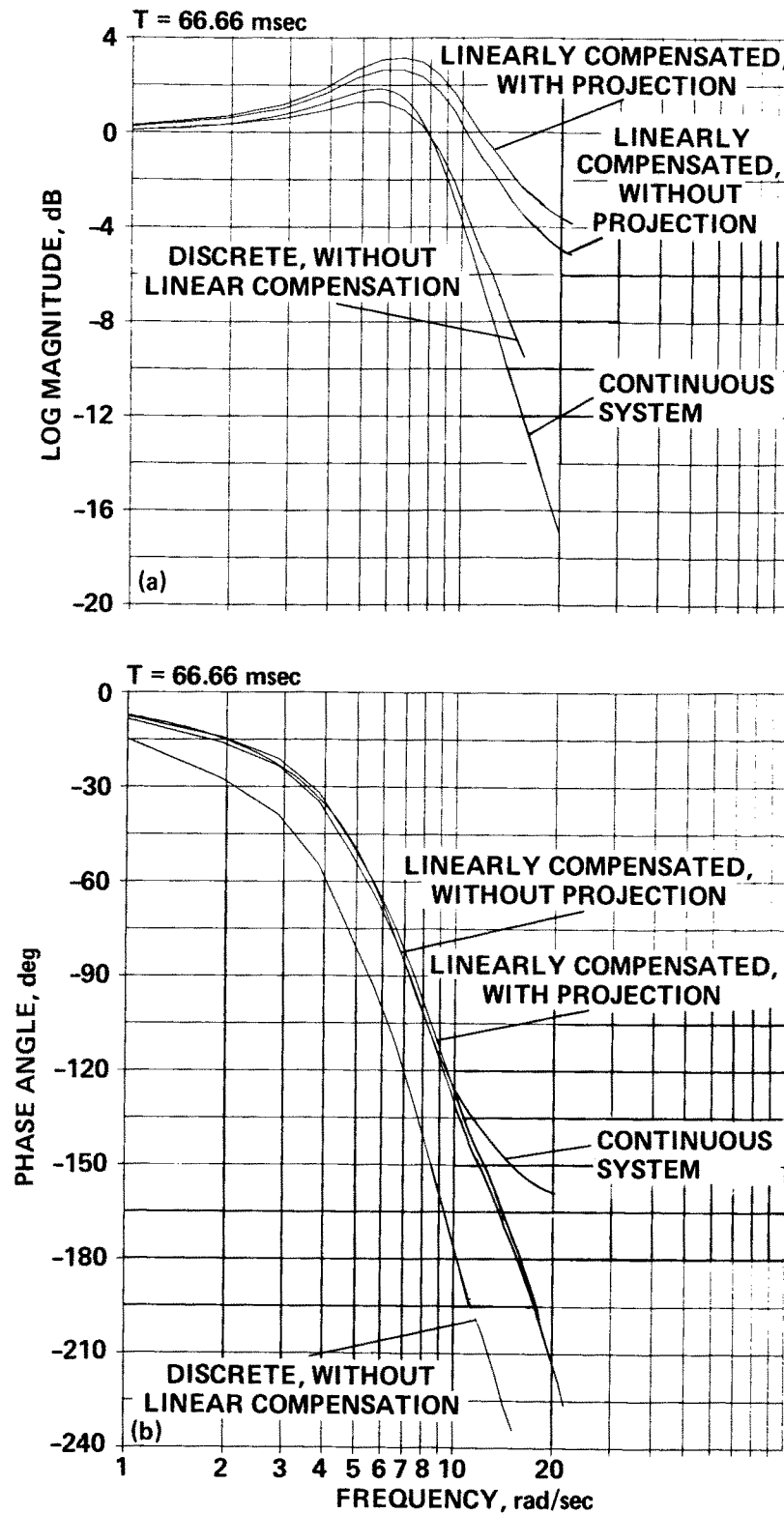
Figure 5.— Transfer function and linear compensation. (a) Magnitude. (b) Phase.

(a)

(b)
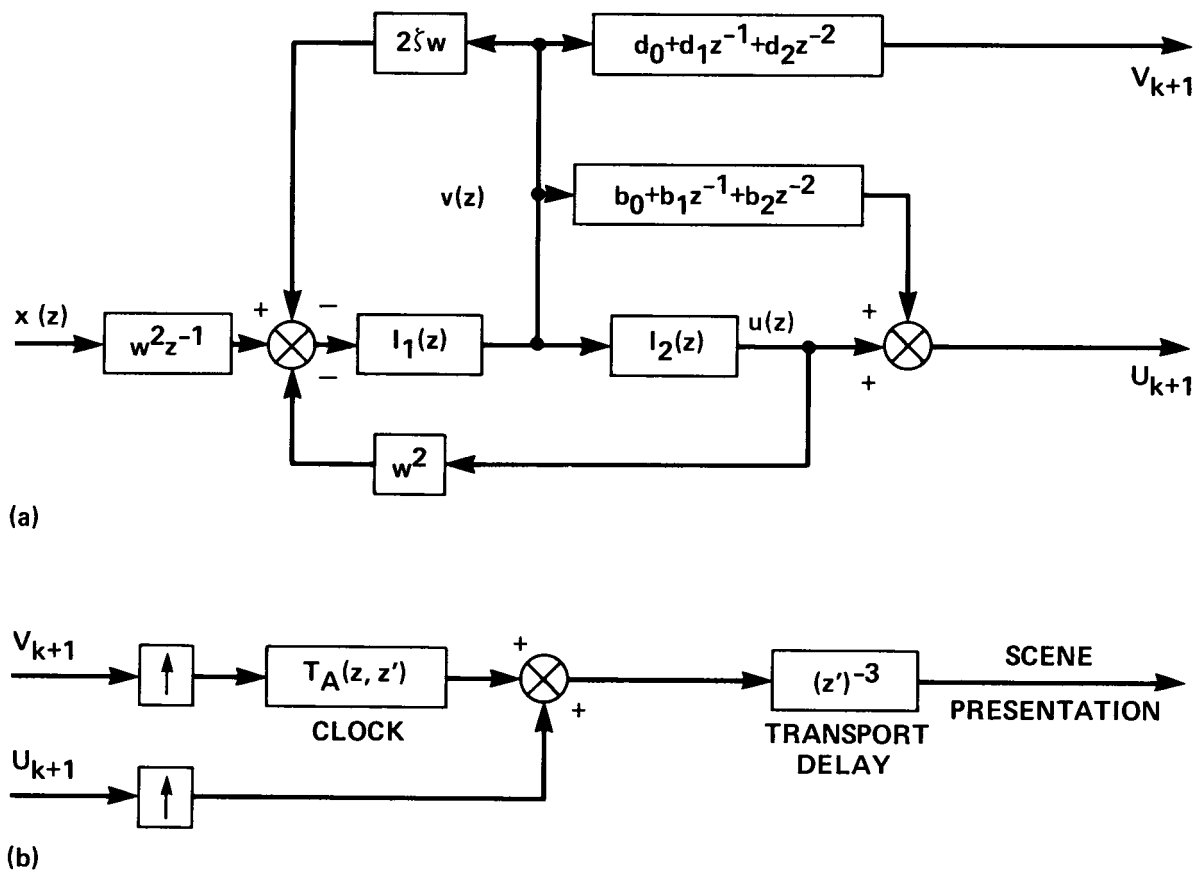
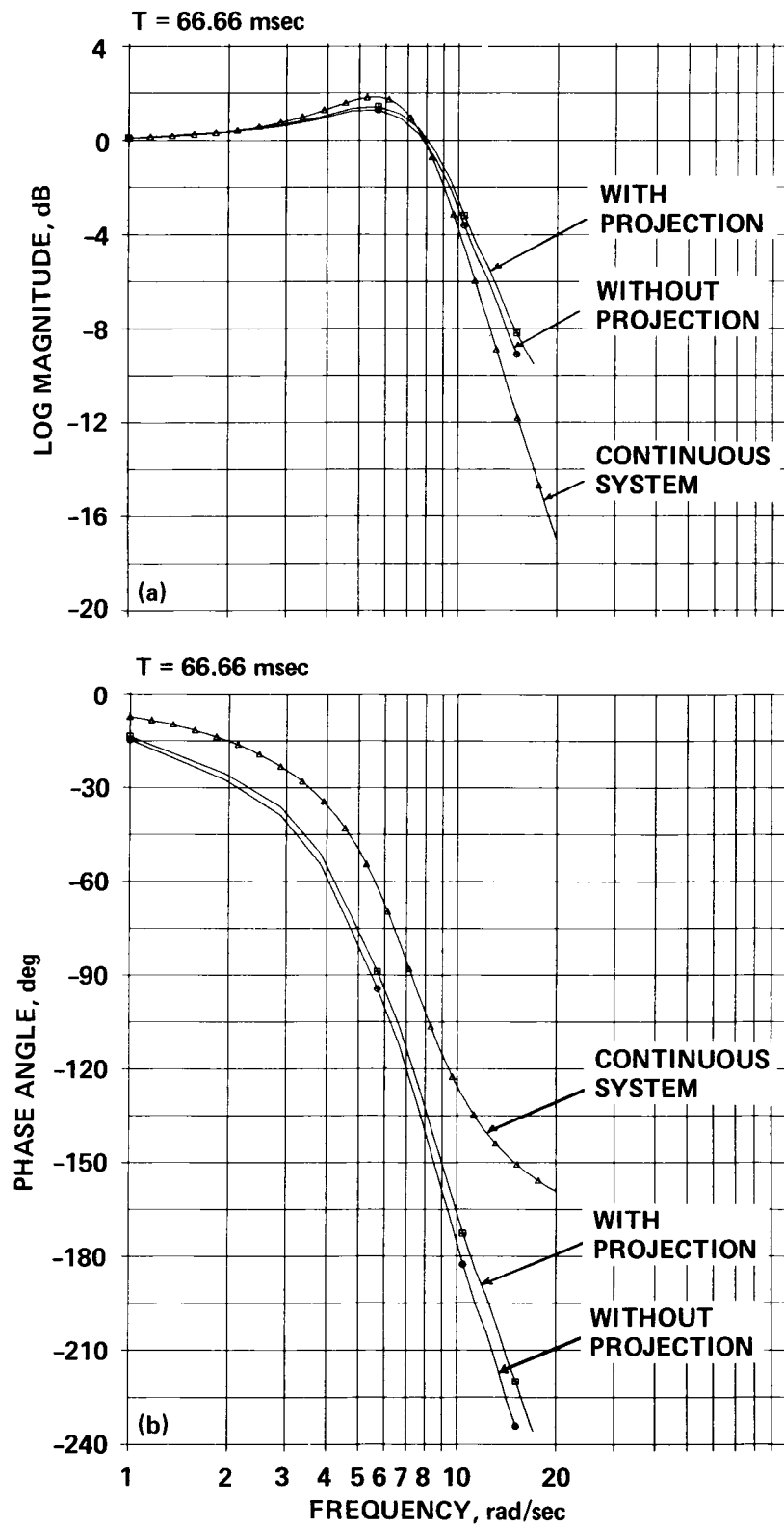Figure 6.— Discrete operations. (a) Mainframe operations at $1/T$ Hz. (b) CGI operations at 30 Hz.

21

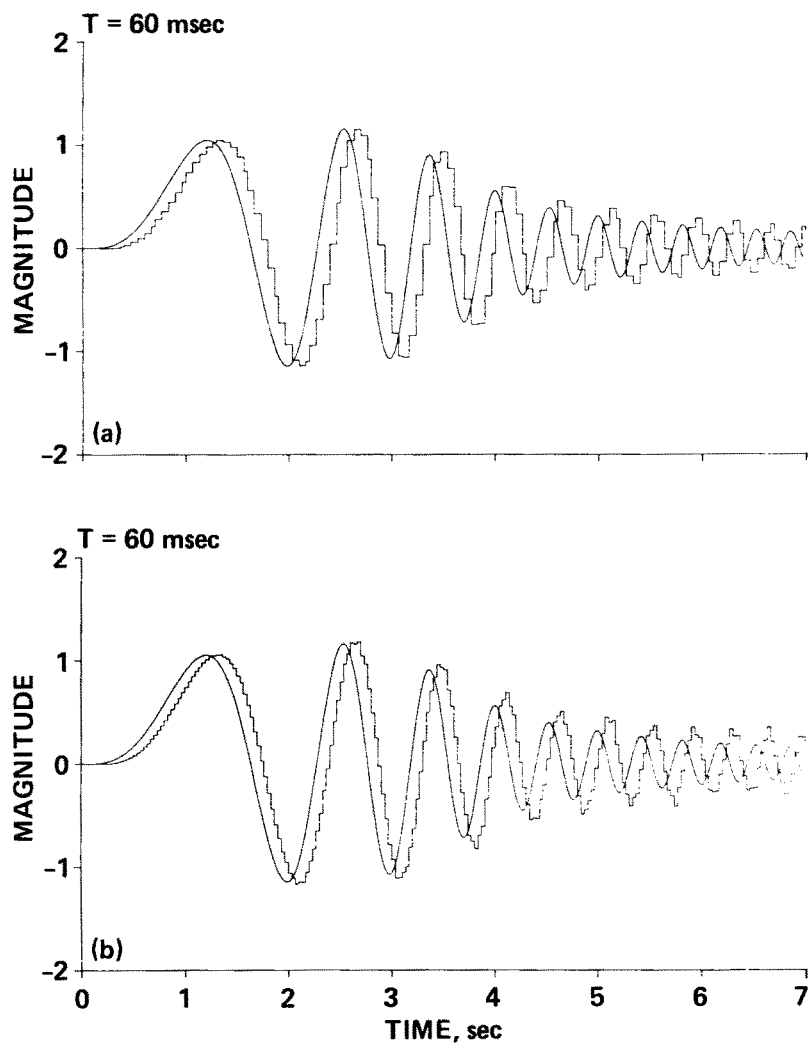Figure 7.— Transfer function without compensation. (a) Magnitude. (b) Phase.

22

Figure 8.— Time history of system without compensation. (a) Without projection. (b) With projection.
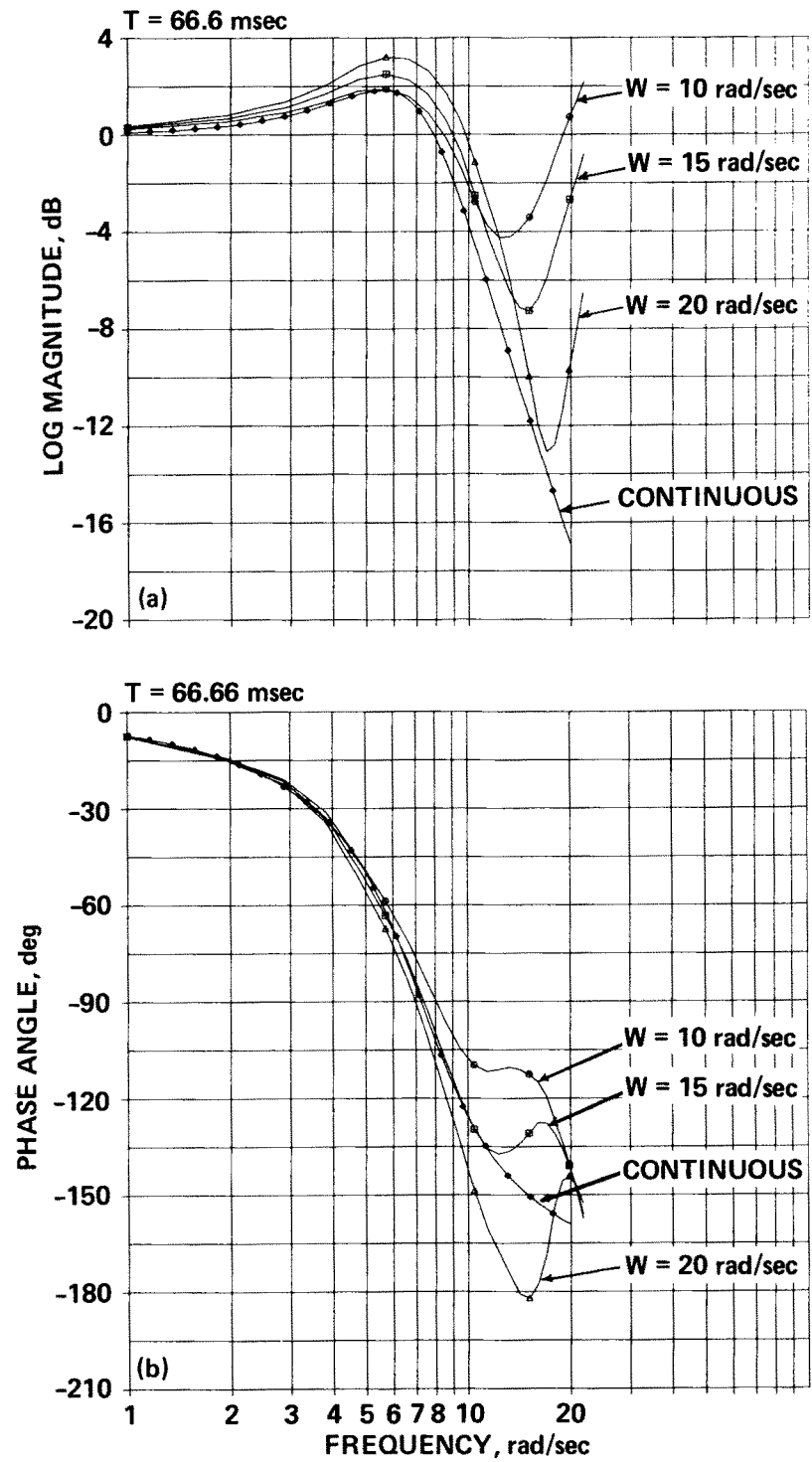
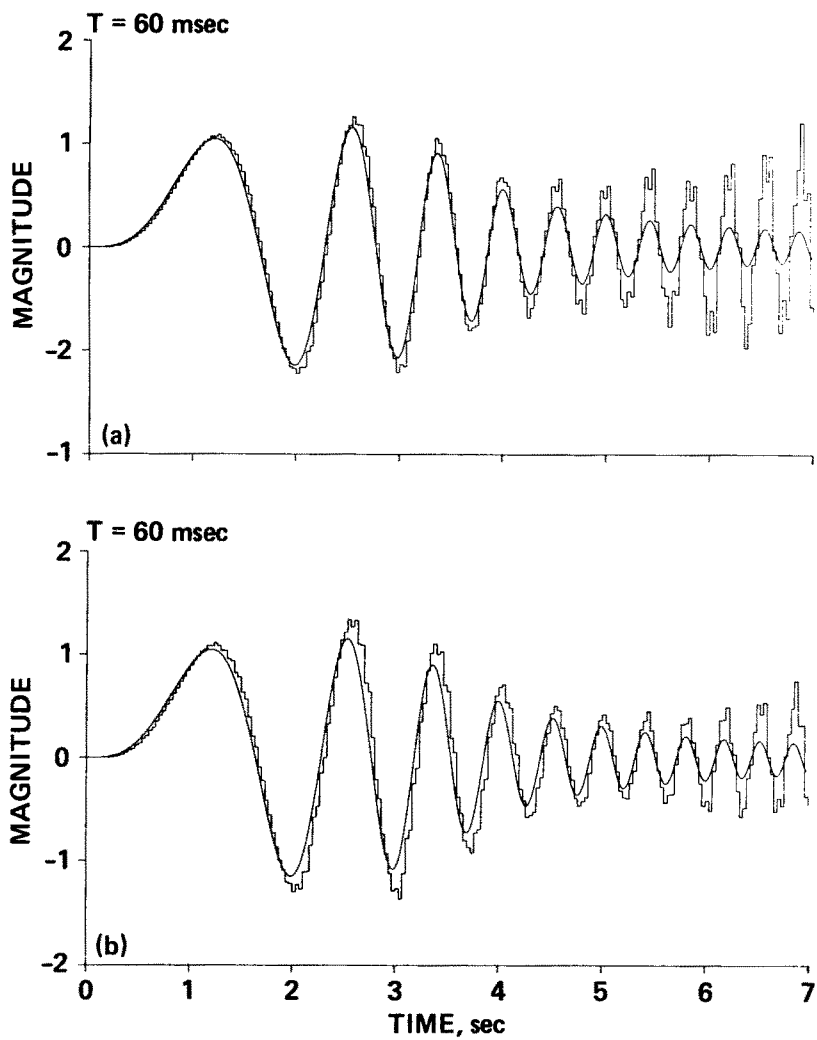Figure 9.— Transfer function with compensation. (a) Magnitude. (b) Phase.

Figure 10.— Time history of system with compensation. (a) Cutoff frequency of 10 rad/sec. (b) Cutoff frequency of 15 rad/sec.
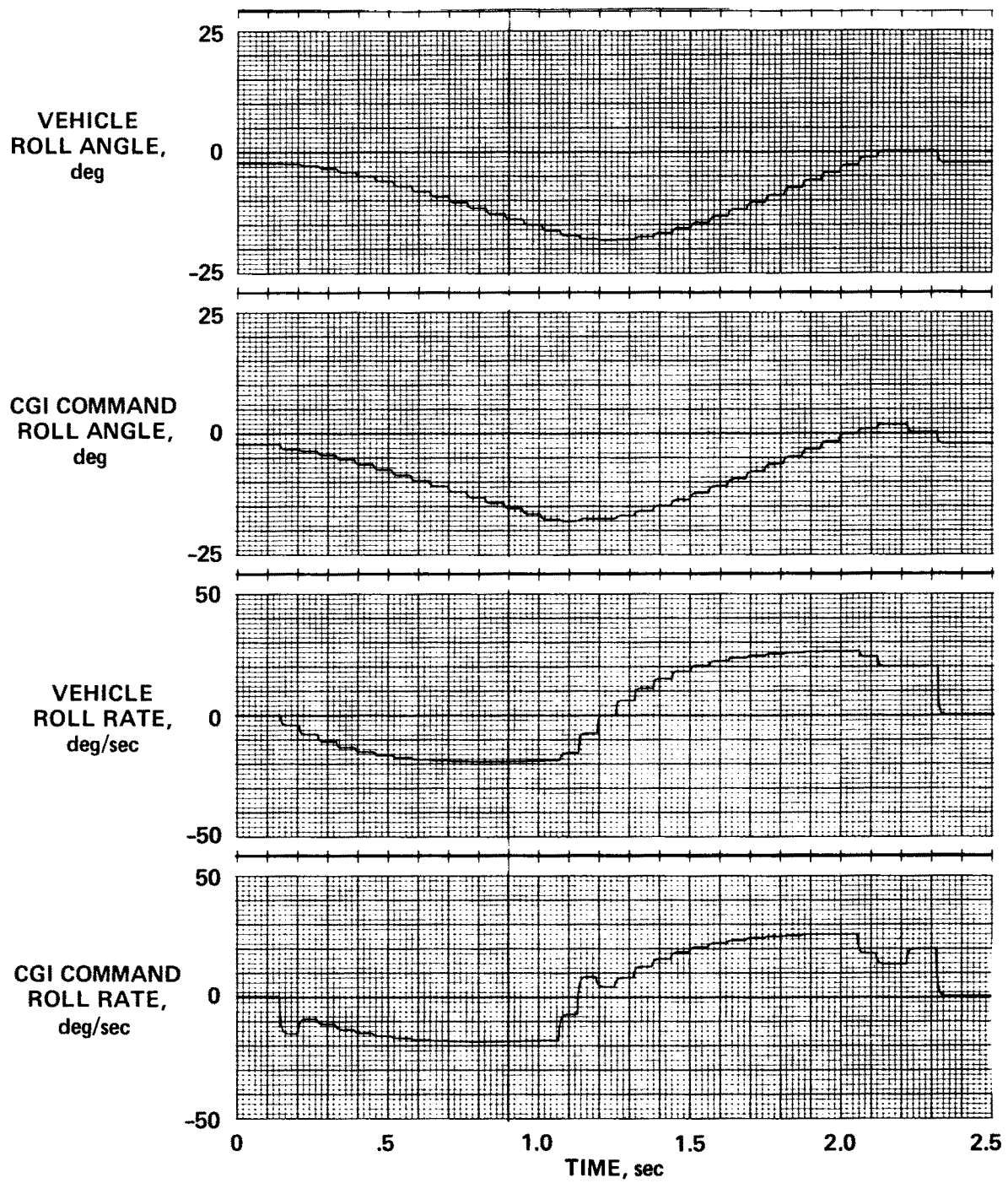
Figure 11 — Typical dynamic check, roll angle and rate with compensated CGI commands.

1. Report No. NASA TM-86703	2. Government Accession No.	3. Recipient's Catalog No.
4. Title and Subtitle CGI DELAY COMPENSATION		5. Report Date January 1986
		6. Performing Organization Code
7. Author(s) Richard E. McFarland		8. Performing Organization Report No. 85168
		10. Work Unit No.
9. Performing Organization Name and Address Ames Research Center Moffett Field, CA 94035		11. Contract or Grant No.
		13. Type of Report and Period Covered Technical Memorandum
12. Sponsoring Agency Name and Address National Aeronautics and Space Administration Washington, DC 20546		14. Sponsoring Agency Code 505-42-71

15. Supplementary Notes

Point of contact: Richard E. McFarland, Ames Research Center, Moffett Field, CA 94035
(415) 694-6171 or FTS 448-6171

16. Abstract

Computer-generated graphics in real-time helicopter simulation produces objectionable scene-presentation time delays. In the flight simulation laboratory at Ames Research Center, it has been determined that these delays have an adverse influence on pilot performance during aggressive tasks such as nap-of-the-Earth (NOE) maneuvers.

Using contemporary equipment, computer-generated image (CGI) time delays are an unavoidable consequence of the operations required for scene generation. However, providing that magnitude distortion at higher frequencies are tolerable, delay compensation is possible over a restricted frequency range. This range, assumed to have an upper limit of perhaps 10 or 15 rad/sec, conforms approximately to the bandwidth associated with helicopter handling qualities research.

A compensation algorithm is introduced here and evaluated in terms of tradeoffs in frequency responses. The algorithm has a discrete basis and accommodates both a large, constant transport delay interval and a periodic delay interval, as associated with asynchronous operations.

17. Key Words (Suggested by Author(s)) Time delay Compensation Real-time simulation Computer-generated graphics Operational bandwidth Asynchronous transfers		18. Distribution Statement Unclassified – Unlimited Subject Category 05	
19. Security Classif. (of this report) Unclassified	20. Security Classif. (of this page) Unclassified	21. No. of Pages 29	22. Price A03